HHS Public Access

Author manuscript

Neuropharmacology. Author manuscript; available in PMC 2020 February 17.

Published in final edited form as:

Neuropharmacology. 2016 August ; 107: 239–250. doi:10.1016/j.neuropharm.2016.03.029.

Stress increases GABAergic neurotransmission in CRF neurons of the central amygdala and bed nucleus stria terminalis

John G. Partridge[a,b,*], **Patrick A. Forcelli**[a,b], **Ruixi Luo**[a], **Jonah M. Cashdan**[c], **Jay Schulkin**[b,d], **Rita J. Valentino**[e], **Stefano Vicini**[a,b]

[a]Department of Pharmacology & Physiology, Georgetown University School of Medicine, Washington, DC 20007, USA

[b]Interdisciplinary Program in Neuroscience, Georgetown University School of Medicine, Washington, DC 20007, USA

[c]Department of Biology, Georgetown University School of Medicine, Washington, DC 20007, USA

[d]Department of Obstetrics & Gynecology, University of Washington, Seattle, WA 98195, USA

[e]Abramson Pediatric Research Center, Children's Hospital of Philadelphia, Philadelphia, PA 19104, USA

Abstract

Corticotrophin Releasing Factor (CRF) is a critical stress-related neuropeptide in major output pathways of the amygdala, including the central nucleus (CeA), and in a key projection target of the CeA, the bed nucleus of the stria terminalis (BnST). While progress has been made in understanding the contributions and characteristics of CRF as a neuropeptide in rodent behavior, little attention has been committed to determine the properties and synaptic physiology of specific populations of CRF-expressing (CRF^+) and non-expressing (CRF^-) neurons in the CeA and BnST. Here, we fill this gap by electrophysiologically characterizing distinct neuronal subtypes in CeA and BnST. Crossing tdTomato or channelrhodopsin-2 (ChR2-YFP) reporter mice to those expressing Cre-recombinase under the CRF promoter allowed us to identify and manipulate CRF^+ and CRF^- neurons in CeA and BnST, the two largest areas with fluorescently labeled neurons in these mice. We optogenetically activated CRF^+ neurons to elicit action potentials or synaptic responses in CRF^+ and CRF^- neurons. We found that GABA is the predominant co-transmitter in CRF^+ neurons within the CeA and BnST. CRF^+ neurons are highly interconnected with CRF^- neurons and to a lesser extent with CRF^+ neurons. CRF^+ and CRF^- neurons differentially express tonic GABA currents. Chronic, unpredictable stress increase the amplitude of evoked IPSCs and connectivity between CRF^+ neurons, but not between CRF^+ and CRF^- neurons in both regions. We propose that reciprocal inhibition of interconnected neurons controls CRF^+ output in these nuclei.

[*]Corresponding author. Department of Pharmacology and Physiology, Basic Science Building, Rm 235, Georgetown University School of Medicine, 3900 Reservoir Rd, Washington, DC 20007, USA. jp374@georgetown.edu (J.G. Partridge).

Author contributions

JGP, PF, JS and SV contributed to the conception and design of the study; JGP, RL, PF, RJV and SV performed the experiments; JGP, JMC, PF, and SV analyzed data and prepared figures; JGP, PF, JS, RJV and SV drafted the manuscript, while RL and JMC edited and revised the manuscript. All authors approved the final version of the manuscript.

Keywords

ChR2; GABA; Chronic unpredictable stress; Corticotropin releasing factor

1. Introduction

Anxiety disorders, the most common of neuropsychiatric conditions, contribute to the etiology of major depression and substance abuse (Kessler et al., 2005). The macrocircuitry controlling fear and anxiety relies crucially on the amygdala, a brain region important for emotional processing (Kim et al., 2013; Luthi and Luscher, 2014), as well as the bed nucleus of the stria terminalis (BnST), a key amygdala output target.

Within the amygdala, the basolateral nucleus (BLA) is comprised of ~90% glutamatergic neurons, whereas the central nucleus (CeA) contains 95% GABAergic medium sized neurons (Marek et al., 2013). A primary output sub-region of the amygdala is the medial CeA (CeM). When the CeM is chemically or electrically excited, autonomic and behavioral responses associated with fear and anxiety via projections to the hypothalamus and brainstem results. The BnST is also considered an essential target of the CeA. It serves a key role in stress responses by receiving inputs from the CeA and then projecting to the paraventricular nucleus of the hypothalamus (PVN), the main regulator of systemic glucocorticoid levels. In addition, the BnST sends both GABAergic and glutamatergic projections to the ventral tegmental area (VTA) and other areas involved in the regulation of anxiety (Jennings et al., 2013; Johansen, 2013).

CRF is a neuropeptide that is particularly enriched in the CeA and BnST. It has received special attention for its role in anxiety, and the hormonal and behavioral response to adversity (Pitts et al., 2009; Schulkin, 2011). In fact, CRF infusion in either region increases heart rate in rats (Nijsen et al., 2001) and causes anxiety-like behavior (Koob and Thatcher-Britton, 1985; Daniels et al., 2004; Sahuque et al., 2006; Davis et al., 2010; Donatti and Leite-Panissi, 2011).

Within the CeA and BnST, GABA is also critical regulator of anxiety-like behaviors, and a well-established contributor to neurophysiological and behavioral phenotypes associated with these states including drug and alcohol consumption (Richter et al., 2000; Hayes et al., 2005; Funk et al., 2006; Lowery-Gionta et al., 2012; Herman et al., 2013b; Silberman and Winder, 2013; Zorrilla et al., 2014; Herman et al., 2015). As reviewed by Gilpin (Gilpin, 2012) increases in local GABA within the CeA are translated to decreased inhibitory tone within CeA target regions, including the BnST. Disinhibition of these target zones is associated with increases in stress and anxiety-like behavior. Consistent with this, microinjection of the $GABA_A$ receptor agonist, muscimol, into the BnST attenuates the response to both conditioned and unconditioned fear-evoking stimuli (Fendt et al., 2003). Moreover, in some species, the CeA provides a CRFergic projection to the BnST (Sakanaka et al., 1986), as well as to lateral hypothalamus, the reticular formation, and parabrachial nuclei. Interestingly, there is a well-established anatomical and functional GABAergic projection from CeA to BnST (Sun and Cassell, 1993; Li et al., 2012). The degree to which

these GABAergic and CRFergic projections overlap remains to be conclusively demonstrated.

Immunohistochemical, in situ hybridization (Day et al., 1999), and single cell PCR data have confirmed overlap and co-expression of markers of GABAergic and CRFergic phenotype in the BnST (Sarkar et al., 2011; Dabrowska et al., 2013). In other brain regions, CRF co-localizes with other neurotransmitter markers, for example, glutamate in the PVN (Hrabovszky et al., 2005; Dabrowska et al., 2013). Co-localization between CRF and other neuropeptide markers (e.g., oxytocin, vasopressin, and neurotensin) has also been reported (Sawchenko et al., 1984) in the PVN, and co-expression with prodynorphin (which also co-localized with GABA) has been described in the CeA (Ma et al., 2003; Marchant et al., 2007). The diversity in CRF co-expression across neuronal types and across brain regions underscores the importance of detailed examination of the functional phenotype of these neurons.

Despite a long history of interest in CRF within the amygdala and BnST, only recently have studies begun to dissect the functional phenotype of CRF neurons in these regions. While a wealth of prior studies have characterized the cytochemical organization of the CRF system in the brain, only the recent availability of *CRF*-specific Cre driver lines have allowed the dissection of the neurophysiology of this neuron population. We chose the *CRF*-CRE transgenic line that has recently been used to characterize the firing properties of CRF^+ neurons in the BnST, CeA (Silberman et al., 2013), PVN (Wamsteeker Cusulin et al., 2013), and hippocampus (Hooper and Maguire, 2016), and displays excellent fidelity as a reporter line (Chen et al., 2015).

The genetic tools described above were used here to test the following hypotheses: 1) CRF^+ neurons display functional, GABAergic synaptic connections with other CRF^+ neurons as well as between CRF^+ and CRF^- neurons and 2) that chronic mild stress would alter the connectivity amongst CRF^+ neurons. We tested these hypotheses through a combination of electrophysiological, pharmacological, and optogenetic approaches to provide a comprehensive characterization of the synaptic networks of CRF^+ neurons in the CeA and BnST. Consistent with our hypothesis, we found that GABA is the primary and functional co-transmitter in CRF^+ neurons, and that the synaptic strength and connectivity is enhanced by chronic stress. The work presented here begins to address the specific role of the synaptic interactions of CRF^+ networks in the control of anxiety.

2. Methods

2.1. Slice preparation, pharmacology and electrophysiology

The strain of transgenic mice examined in this study, to genetically identify or activate fluorescent neurons was JAX stock #012704 (B6(Cg)-$CRF^{tm1(cre)Zjh}$/J) (Silberman et al., 2013; Wamsteeker Cusulin et al., 2013). The *CRF*-ires-Cre allele contains Cre recombinase in the 3′ UTR of the *CRF* locus allowing the expression of Cre directed by the endogenous *CRF* promoters/enhancers. Hemizygous mice were bred with either tdTomato "*rosa26* floxed-stop", Ai14, Jackson Laboratory (Bar Harbor, ME) Stock # 007914 (Madisen et al., 2010) or ChR2H134R-EYFP, Ai32, Jackson Laboratory Stock # 012569 "reporter" mice

(Madisen et al., 2012). These mice display the typical patterns of CRF^{+} labeling throughout the CNS (Taniguchi et al., 2011; Chen et al., 2015). Acute slice preparations were prepared as described previously (Adedoyin et al., 2010; Partridge et al., 2014). Male or female mice were sacrificed by decapitation in agreement with the guidelines of the AMVA Panel on Euthanasia and the Georgetown University animal care and use committee. Following dissection, brains were rapidly placed in ice-cold slicing solution containing (in mM): NaCl (85), KCl (2.5), $CaCl_2$ (1), $MgCl_2$ (4), NaH_2PO_4 (1), $NaHCO_3$ (25), glucose (25), and sucrose (75), osmolarity 325 mOsm. Recordings from 250 μm coronal slices containing the BnST or amygdala were performed in artificial cerebrospinal fluid (aCSF) containing (in mM): NaCl (124), $NaHCO_3$ (26), dextrose (10), KCl (4.5), $CaCl_2$ (2.0), Na_2HPO_4 (1.2) and $MgCl_2$ (1), osmolarity 325 mOsm. Epifluorescent excitation of the tissue allowed neuron selection using a 60× water immersion objective. Recording pipettes were filled with either potassium chloride (KCl) or potassium gluconate (Kgluc) solutions. The KCl solution contained (in mM): KCl (145); HEPES (10), EGTA (5), ATP·Mg (5), and GTP·Na (0.2), osmolarity 305 mOsm; adjusted to pH ~7.20 with KOH. For Kgluc-based internal solutions, KCl was replaced with (145 mM) potassium gluconate. Stock solutions of bicuculline methobromide (BIC), tetrodotoxin (TTX), 2,3-dioxo-6-nitro-1,2,3,4-tetrahydrobenzo[f]quinoxaline-7-sulfonamide (NBQX), all from Abcam Biochemical (Cambridge, MA) were prepared in water and diluted 1:1000 in aCSF.

Recording electrodes were made from glass capillary tubes (Drummond Scientific Company, Broomall, PA, Cat. #5-000-2050) using a vertical heating puller (PP-83, Narishige, Tokyo, Japan). Pipettes with tip resistances between 4 and 6 MΩ were used for all recordings. Patch clamp recordings were performed using a MultiClamp 700B amplifier while signals were low-pass filtered at 2 kHz, sampled at 5 kHz and acquired with a Digidata 1440A (Molecular Devices, Sunnyvale, CA) on a Dell OptiPlex 990 PC.

2.2. Morphological studies

Confocal z-stacks (0.5–1.3 μm in thickness) were collected with a ThorLabs Imaging resonance laser scanning confocal (Sterling, VA) equipped with a 488 nm/561 argon laser integrated on a Nikon Eclipse FN1 upright microscope. “z-projection” stacks were prepared with Image J software (v1.47n, Bethesda, MD).

2.3. Immunohistochemistry

Brain sections were prepared from adult male or female mice aged ~3 months. After isoflurane anesthesia, animals were placed on an elevated surgical board and a Y-incision in the thoracic-abdominal region was made to expose the heart. A needle was inserted into the left ventricle, clamped in place, and connected to a pumping perfusion system. The perfusion was initiated with a 200 mL 0.1 M phosphate-buffered saline wash (PBS) pH 7.4, followed by a 200 mL phosphate-buffered paraformaldehyde fixative (0.1 M and 4% respectively, pH 7.4). The brains were then removed and stored overnight in the phosphate-buffered paraformaldehyde fixative before being transferred to a 20% sucrose solution (PBS/20% sucrose).

Immunostaining was performed as in Valentino et al. (Valentino et al., 1992). Frozen 30 μm coronal sections were cut on a cryostat and collected in a series of 4 wells in 0.1 M PBS. Sections were incubated in 0.75% H_2O_2 for 20 min and then rinsed 3 × 10 min with PBS containing 0.3% Triton-X and 0.04% bovine serum albumin (PBS-TX-BSA). Sections were incubated with either rabbit anti-CRF (1:1000, Dr. Wylie Vale, the Salk Institute, La Jolla, CA), rabbit anti-GABA (1:1000, Sigma) or mouse monoclonal anti-GAD67 (1:500, MAB5406, Chemicon-Millipore, Billerica, MA), in PBS-TX-BSA and 0.1% sodium azide for 48–72 h at 4 °C. Following three PBS-TX-BSA rinses (10 min each), sections were incubated in secondary antibodies for 90 min at room temperature. For immunohistochemical processing of sections from *crf*;tdTomato mice, secondary antibodies were donkey anti-rabbit conjugated to FITC (Jackson Immuno Research, West Grove, PA). Sections were then rinsed in PBS, mounted, and cover-slipped with Fluoromount G (SouthernBiotech, Birmingham, AL). For confocal imaging, 2-channel resonance laser scanning confocal was used for excitation of endogenous tdTomato or FITC fluorescence. 1 μm thick z-stack images (1024 × 1024 pixels) were processed with ImageJ software and presented as a composite image of 12–20 z-stacks. Immuno-reactive neurons for GAD67 from representative sections containing either the CeA or BnST (24 sections from 3 adult male mice) were counted and analyzed for dual-labeling. Co-localization of immunostaining overlap was performed by manually tracing regions of interest corresponding to the cell bodies of neurons expressing tdTomato with Image J in all focal planes. Counts of neurons co-localizing the two markers were expressed as a percentage of the total number of neurons.

2.4. Optogenetics and slice recording

Coronal slices from Cre-dependent ChR2-YFP “reporter” mice were acutely prepared from postnatal day 17 to adult animals (>PD300). Slices were excited with 488 nm light from an argon laser source at 3–8% power or from X-Cite 120 LED (Excelitas Technologies, Waltham, MA) with maximal light intensity adjusted to prevent loss of voltage-clamp (V_{hold} = −70 mV). We assessed maximal light evoked postsynaptic currents in response to light applications greater than 100 ms to avoid the variability that we observed with shorter light pulse duration due to a variety of uncontrolled variables such as the time constant of the presynaptic cells and changes in release probability with repeated stimulations. All experiments were performed at room temperature (22–24 °C) with the exception of a subset performed at elevated temperature (30–32 °C) in attempts to observe endogenous CRF release. Access resistance was monitored periodically with a 15 ms, −5 mV test pulse applied 30 ms before the onset of light stimulation. Those neurons in which the access resistance changed by >10% were discarded from the final population of cells for statistical analyses. Light stimulations did not alter the passive membrane properties as assessed by the test pulse. The following compounds were tested in optogenetic experiments at the following concentrations in micromolar (μM): BIC (25), GABAzine (10), NBQX (5), or antalarmin (25). All these agents were purchased from Sigma-Aldrich (St. Louis, MO).

2.5. Patch clamp analysis

Standard electrophysiological analysis was conducted to measure the mean peak response obtained by averaging the largest IPSC across 20 trials separated by 10 s intervals. Data

collected were derived from 26 mice with an average of 8 cells per mouse (range 3–24 cells). The rate of action potentials was determined via threshold detection software (Clampfit v10.4, Molecular Devices LLC, Sunnyvale, CA). Spontaneous inhibitory postsynaptic currents (sIPSCs) were analyzed with mini Analysis 6.0.3 (Synatosoft Inc., Fort Lee, NJ). AMPA-mediated sEPSCs were identified by their rapid decay kinetics (<7 ms) and were excluded from the analysis. sIPSC frequency assessment was based on at least 100 events in each cell studied.

2.6. Chronic unpredictable stress paradigm

This protocol consisted of a once daily stressor from the following three paradigms given randomly over a 5–7 day time period: 1) cold stress: prolonged exposure to 4 °C cold room for 120 min each in novel cage; 2) restraint stress: 1 h placement of mouse in a Falcon 50 mL conical tube with custom made air holes for air circulation (Fisher Scientific); or 3) foot shock stress: randomly variable between 0.5s and 1s in duration, 10 × 0.5–1.0 mA shocks given randomly over at 90 s time interval (Schweizer et al., 2009). Electrophysiology experiments were performed 16–40 h after the last stressor, a period during which we found behavioral signs of anxiety caused by chronic stress (see below).

2.7. Behavioral assessment of chronic unpredictable stress effects

B6129SF2/J wild type mice (JAX strain # 101045), selected to approximate the genetic background of F1 offspring resulting from our crosses of *CRF*-Cre and reporter lines, were used for behavioral verification of the efficacy of our chronic stress paradigm.

Two days after chronic stress, animals were tested for anxiety-like behavior in the open field, followed two weeks later by habituation of the acoustic startle response. We selected these two time points to demonstrate long-lasting effects of chronic stress in our animals. For open field testing, mice were placed in the center of a novel Plexiglas chamber and tracked using ANYmaze software (Stoelting) and the time in the center vs periphery of the chamber was calculated over the 5 min test. For habituation of the acoustic startle response, animals were tested in the SRLab startle system (San Diego Instruments) and presented with a series of five 120 dB white noise pulses, followed by prepulse inhibition trials as previously described (Washington et al., 2012; Wurzman et al., 2015), followed by another five 120 dB white noise pulses. Habituation of startle was calculated by taking the average startle response to the last five trials divided by the average startle response to the first five trials.

2.8. Statistics

Unpaired Student’s t-tests were used to investigate relationships between control and treated conditions unless otherwise indicated. In some cases, we employed Mann-Whitney-U tests (non-parametric) when sample size was lower, normality was in question, or variance was unequal. Paired Student’s t-tests were used for two-sample comparisons within the same neuron. Statistics were conducted with GraphPad Prism (La Jolla, CA) or Excel software. All data values in text and figures are presented as mean ± SEM. All figures were prepared with ClampFit, ImageJ, Powerpoint, Igor or Excel software. While both age and sex are biological variables of interest, they were not of primary concern for this manuscript. Thus, we collapsed across age and sex to maximize statistical power for the comparisons of

primary interest, e.g., stressed vs non-stressed. This approach is supported by the finding of Sterrenburg and colleagues, who found similar levels of cFos responsivity [a presumptive marker of neuronal activation] in male and female rats after stressors, despite sex differences in CRF and plasma stress responses (Sterrenburg et al., 2012). We were not able to make a comparison between young and old or male and female animals as all of these analyses were underpowered when assessed by post-hoc power analysis.

3. Results

3.1. CRF expressing neurons in the BnST and CeA

Mice that express Cre recombinase in neurons directed by the promoter for the *crf* gene have been recently used to study CRF immunopositive neurons in the BnST and CeA (Silberman et al., 2013), the PVN (Wamsteeker Cusulin et al., 2013) and the olfactory bulb (Huang et al., 2013). To confirm and extend these results, we performed electrophysiology and immunohistochemistry on genetically identified CRF neurons located in BnST and CeA. To analyze the properties of CRF neurons we investigated mice that express tdTomato red fluorescence in these neurons. Fig. 1 compares a horizontal slice (Fig. 1A) with coronal slices (Fig. 1B–C) at low magnification (2×). In the horizontal slice *crf*;tdTomato expressing neurons are seen at low density throughout the cortex and hippocampus. However bright clusters of high neuronal densities are seen in extended areas corresponding to the CeA and the BnST. Orthogonal coronal slices at two distinct sections (Fig. 1B–C) clearly reveal identifiable clusters of high CRF^+ neuron density. The BnST (Fig. 1B) is located in the more rostral section containing the anterior commissure, which was used to identify the location of the BnST. The CeA (Fig. 1C) is displayed in a more caudal section. High power (60×) photomicrographs of these neurons, below the low power images, show that they are heterogeneous in shape and size in the BnST but more medium sized with spiny dendrites in the CeA. Immunostaining with antibodies against CRF revealed co-expression of somatic tdTomato and CRF antigen immunoreactivity as seen in Fig. 1D and reported for CRF neurons of the PVN (Wamsteeker Cusulin et al., 2013) BnST, amygdala and hippocampus (Chen et al., 2015). CRF immunoreactivity and tdTomato expression extensively co-localized in 480 neurons in 3 sections each analyzed from 2 mice. CRH immunoreactivity was observed in 83% of the tdTomato neurons. Conversely, nearly all soma containing CRH co-expressed tdTomato (98%).

Current clamp recordings from tdTomato expressing neurons (CRF^+) in BnST (Fig. 1E) or CeA (Fig. 1F) matched the reported hyperpolarized and largely variable resting membrane potential in BnST and CeA neurons, respectively (Silberman et al., 2013). In addition, compatible with that detailed study, the action potential firing pattern in response to current injection was characterized by a delay to first spike and the presence of inward rectification for CeA neurons that responded occasionally with burst firing to depolarizing current injection. Similar types of CeA CRF^+ neurons were reported in the study of Silberman et al. (2013). This phenotype matches one of several subtypes of unidentified CeA neurons characterized by the response to depolarizing current injections (Lopez de Armentia and Sah, 2004; Chieng et al., 2006; Herman et al., 2013a). Non-labeled neurons in CeA were of

two major sub-types, one with striatal projection neuron-like firing (Luo et al., 2013) and the other with a somatostatin/neuropeptide Y-like neuron firing (Ibanez-Sandoval et al., 2011).

3.2. Optogenetic activation of crf;ChR2-YFP neurons

To further characterize the synaptic physiology of CRF^+ neurons in the BnST and CeA, optogenetic techniques were used to manipulate their activity in slices from *CRF*;ChR2-YFP expressing mice. As shown in the example trace in Fig. 2A, repetitive pulses of blue light consistently evoked sustained action potential firing in cell attached mode from a CRF^+ neuron in the CeA. For the subset of cells in which we did this experiment, similar results were seen in 13/13 CRF^+ BnST neurons and 19/19 CRF^+ CeA neurons. The majority of our recordings in the BnST were performed in the ventral area of this large nucleus. However, the CRF neurons within this area were visualized across several sub-nuclei within the ventral BnST. We therefore pooled data from these areas to maximize the number of neurons from which data were collected.

Upon whole cell current clamp recordings, blue light activation of CRF^+ neurons induced depolarization that, when sufficiently large, were capable of triggering individual or repeated action potentials as in the example CeA neuron shown in Fig. 2B. We then used voltage clamp recordings (V_{hold} = −70 mV), as shown in the traces in Fig. 2C, to determine the extent and shape of optogenetically activated currents from CRF^+ neurons. In this configuration, we consistently evoked inward currents that activated and inactivated in a reliable manner with the duration of the light pulse.

When the light evoked response from CRF^+ neurons was examined in more detail by recording with high $[Cl]_i$ we occasionally observed fast postsynaptic current (PSC)-like events stochastically superimposed on the larger ChR2 current (Fig. 2C, left). We detected these types of events in 4 of 14 BnST CRF^+ neurons and 11 of 28 CeA CRF^+ neurons. This is graphically illustrated in Fig. 2D. Upon application of 25 μM bicuculline (BIC), the PSC-like events were greatly reduced and a more isolated ChR2 current remained (Fig. 2C, right). The amplitude of the BIC insensitive current was on average 157 ± 27 pA in 14 BnST CRF^+ neurons and 237 ± 41 pA in 28 CeA CRF^+ neurons. When an averaged ChR2 current (from within each individual cell) was subtracted from the total current response we were able to study light-evoked fast PSCs in CRF^+ neurons (see Fig. 2E). The light-evoked PSCs may be due to glutamate release from other CRF^+ neurons; either directly on the recorded CRF^+ neuron, or via polysynaptic pathways by intermediary neurons. Therefore, we tested these hypotheses with application of the AMPA receptor antagonist NBQX (5–10 μM). The evoked synaptic responses were unaltered in 4/4 CRF^+ neurons in the BnST and 5/5 CRF^+ neurons in the CeA where we observed light evoked synaptic responses. These results demonstrate that CRF^+ neurons release GABA upon optogenetic stimulation, and suggest that GABA together with CRF is the major co-transmitter in these cells.

We next turned our attention on CRF^- neurons and repeated the experiments described above. Initial current clamp recordings from unidentified CRF^- neurons in BnST were quite variable (example in Fig. 3A). Spiking patterns and resting membrane potential values were unpredictable and only partially matched the three major types of BnST neurons previously reported in rats (Hammack et al., 2007). In contrast, several CRF^- neurons located in the

CeA were found to have non-accommodating regular firing pattern with inward rectification similar to those reported in striatal spiny projection neurons (Luo et al., 2013). As shown in Fig. 3B, in additional CRF^{-} neurons located in the CeA, we observed burst firing typical of somatostatin expressing neurons (Taniguchi et al., 2011).

When light evoked responses were studied in more detail from CRF^{-} neurons, while recording with high $[Cl]_i$, we frequently observed fast inward currents that resembled IPSCs (Fig. 3C–D). In both BnST (Fig. 3C) and CeA (Fig. 3D) the evoked currents were stochastic when observing the peak amplitude. Light evoked PSCs were seen in 18 of 45 BnST CRF^{-} neurons and 22 of 30 CeA CRF^{-} neurons. As in CRF^{+} neurons, this is graphically illustrated in Fig. 3E. To ascertain the type of neurotransmitter receptor mediating the light evoked currents, we focally applied NBQX (5 μM). This failed to significantly alter the synaptic response in 7/7 CRF^{-} neurons in BnST and 9/9 CRF^{-} neurons in the CeA (Examples in Fig. 3C from CRF^{-} lacking neurons). The nature of the light-evoked PSCs was investigated further with $GABA_A$ receptor antagonists. In both the BnST (Fig. 3C) and the CeA (Fig. 3D), BIC (25 μM) abolished the PSCs (n = 8/9 CRF^{-} cells in BnST, n = 10/14 CRF^{-} cells CeA). This is summarized in Fig. 3F. Comparable results were seen with GABAzine (10 μM, not shown). To determine if the evoked current was action potential mediated we tested the effects of a voltage-gated sodium channel blocker. TTX (500 nM) abolished the current in all 6 neurons tested in this condition. These data, taken together suggest that activation of CRF^{+} neurons (or terminals) in BnST and CeA release GABA that produce IPSCs in target neurons.

To support these electrophysiological observations, we performed immunohistochemical studies using the *crf*;tdTomato strain and antibodies which detect GABA (Valentino et al., 2001) or GAD67 (Dabrowska et al., 2013). As shown in Fig. 3G, the majority of putative CRF neurons ($tdTomato^{+}$) in the CeL were co-labeled by anti-GABA antibodies. Analysis of 200 neurons from 6 sections showed that in CeL 4.0± 2.3% of tdTomato positive cells did not stain with the GABA markers and 18± 7% of GABA or GABAergic neurons did not co-localize with tdTomato expression. In contrast, in 50 neurons from 5 sections of CeM we observed 40± 18% of tdTomato positive cells that did not stain with the antibody for GABA markers and 65± 12% of GABAergic neurons that did not express td-Tomato. Control sections which lacked primary antibodies to GABA did not label any structures. Dual-immunofluorescence experiments in BnST have revealed that 95% of CRF^{+} neurons co-localized GAD67 but the majority of $GAD67^{+}$ neurons do not co-localize CRF (Dabrowska et al., 2013).

3.3. Tonic GABA conductance in BnST and CeA neurons

To investigate the occurrence of tonic activation of $GABA_A$ receptors in CRF^{-} and CRF^{+} neurons in the BnST and CeA we studied the action of a selective $GABA_A$ antagonist on holding current values. Fig. 4A shows on a slow time course the effect of BIC on holding currents in voltage clamp recordings from CRF^{-} or CRF^{+} neurons. In the BnST, BIC unmasked a current of 18.4 ± 4.6 pA in CRF^{-} neurons (n = 19) while this value averaged 3.5 ± 1.1 pA in CRF^{+} neurons (n = 14, Fig. 4B). CRF^{-} neurons in CeA were also more sensitive to the effect of BIC (10.1 ± 1.1 pA, n = 22) than CRF^{+} neurons (5.9 ± 1.3 pA, n = 14, Fig.

4B). Thus in both structures, BIC unmasked significantly larger tonic current in the CRF^{-} neurons as compared to the CRF^{+} neurons (BnST and CeA Mann-Whitney, $p < 0.05$). To extend this finding we used a pharmacological tool to probe the "extra-synaptic" pool of $GABA_A$ receptors. As the δ subunit is enriched in extra-synaptic $GABA_A$ receptors we used the δ preferring agonist THIP (1 μM). In 9 CRF^{-} neurons from CeA, THIP evoked an average inward current of 22.5 ± 5.2 pA while in 6 CRF^{+} neurons, average THIP current was 3.7 ± 1.8 pA ($p < 0.005$, Mann Whitney test). In 5 CRF^{-} neurons from BnST, THIP evoked an average inward current of 48.4 ± 20.6 pA while in 5 CRF^{+} neurons, average THIP current was 2.9 ± 1.4 pA ($p < 0.008$, Mann Whitney test). These data are reported in Fig. 4C.

3.4. Chronic unpredictable stress induces anxiety-like behavior and affects synaptic connectivity in CRF^{+} neurons in CeA and BnST

Because stress has been shown to modulate the CRF system (Lightman and Young, 1988; Merlo Pich et al., 1995; Sandi et al., 2008), resulting in behavioral states consistent with anxiety in animal models, and because chronic stress has been shown to modulate synaptic transmission within the amygdala (Padival et al., 2013; Liu et al., 2014; Masneuf et al., 2014), we next aimed to test the hypothesis that chronic, unpredictable stress (CUS) alters the physiology of CRF^{+} neurons in CeA and BnST.

As shown in Fig. 5, CUS resulted in a significant decrease in time spent in the center of an open field task, consistent with an anxiety-like response (Mann Whitney U = 22, P = 0.0108). This effect was detected 48 h after the final stressor. To determine if an enduring pro-anxiety state was induced by our manipulations, we examined the habituation of acoustic startle response 14 days after the last stressor. We found that animals subjected to CUS displayed reduced habitation as compared to non-stressed control animals (Fig. 5B; Mann Whitney-U = 17, P = 0.043). These data provide behavioral validation for the CUS paradigm, which we subsequently employed in *crf*;ChR2-YFP mice in order to examine synaptic function.

We compared the effects of CUS on light evoked responses from CRF^{-} and CRF^{+} neurons in the BnST and CeA from *crf*;ChR2-YFP mice. As shown in Fig. 5C, repetitive IPSCs were evoked by light stimuli. We used longer light stimuli (400 ms) to increase our ability to detect peak light evoked responses in control vs stressed animals. Fig. 5D summarizes the average peak response to light activation from CRF^{-} and CRF^{+} neurons in the CeA. The average peak response increased only in CRF^{+} neurons. We did not detect any significant effect in synaptically mediated responses under control and stress conditions in CRF^{-} neuron in the CeA (Fig. 5D). Moreover, neither the resting membrane potential nor the passive membrane properties of CRF^{-} or CRF^{+} neurons in either region was modified by CUS. Finally, as shown in Fig. 5E, after CUS we found a significant increase (X^2 test) in the proportion of CRF^{+} neurons that displayed light-evoked synaptic currents. By contrast, stress failed to alter the percent of CRF^{-} neurons with light evoked IPSCs in both BnST and CeA and the persistence of the light response.

3.5. The lack of an effect of a CRF R1 antagonist on IPSCs amplitude and sIPSC frequency in control vs stressed mice

To investigate the possibility that light evokes co-release of GABA and CRF from CRF^+ neurons in the BnST and CeA after CUS, we studied the action of a CRF receptor R1 preferring antagonist, antalarmin (Habib et al., 2000; Oberlander and Henderson, 2012) in CRF^- neurons (Fig. 6A–D). In this subset of experiments the peak PSC response to prolonged light activation, was 60 ± 18 pA (n = 7 BnST neurons) and 274 ± 147 pA (n = 9, CeA neurons). During perfusion of aCSF with 25 μM antalarmin the response was 52 ± 15 pA and 258 ± 123 pA for BnST and CeA neurons, respectively (p = 0.69, paired *t*-test). In slices originating from stressed animals, the averaged peak PSC were 243 ± 129 pA (n = 6 BnST neurons) and 116 ± 38 pA (n = 15 CeA neurons). During perfusion with antalarmin the response was 198 ± 101 pA and 97 ± 33 pA for BnST and CeA neurons, respectively (p = 0.23, paired *t*-test). Statistical comparison with two-way repeated measures analysis of variance (ANOVA) failed to reveal any significant changes due to application of 25 μM antalarmin (Fig. 6A,B). This suggests that if co-release of CRF and GABA occurs with light, it did not acutely change the GABA response in target CRF^- neurons.

CRF acting through the CRF R1 was shown to increase the frequency of sIPSCs, leading to inhibition of postsynaptic dorsolateral BnST neurons (Oberlander and Henderson, 2012) and CeA neurons (Nie et al., 2009). Therefore we measured the occurrence of sIPSCs in CRF^- and CRF^+ neurons in the BnST and CeA from control mice and mice exposed to CUS (Fig. 6C,D). In control mice, we found that the sIPSC frequency in CRF^- neurons was 1.05 ± 0.26 Hz (n = 12 BnST neurons) and 1.07 ± 0.21 Hz (n = 16 CeA neurons). During perfusion with antalarmin, the frequency became 0.78 ± 0.23 Hz and 0.86 ± 0.17 Hz for BnST and CeA neurons, respectively. In the CUS group, the sIPSC frequency was 1.81 ± 0.40 Hz (n = 10 CRF^- neurons in BnST) and 0.92 ± 0.25 Hz (n = 12 CeA CRF^- neurons). During perfusion with antalarmin the frequency became 1.54 ± 0.33 Hz and 0.80 ± 0.20 Hz for BnST and CeA neurons respectively. Statistical comparisons failed to reveal any significant changes due to either stress or CRF R1 antagonist application (Fig. 6C,D). Further, sIPSCs were not significantly different between CRF^- and CRF^+ neurons in BnST and CeA (not shown). Finally, the effects of stress and antalarmin in CRF^+ neurons were also not significant in both areas.

Because we saw a lack of an effect of the receptor antagonist, we also tested the hypothesis that higher recording temperatures could affect the release of CRF from optogenetically driven neurons. In a separate series of experiments we performed at elevated temperatures (30–32 °C), we also failed to see an effect of 25 μM antalarmin on the frequency or amplitude of sIPSCs in 4 cells tested. Further, antalarmin did not modulate the amplitude of light evoked responses from control mice. We tested the effects of 2 different light stimulation frequencies (8.3 vs 50 Hz) as higher frequency stimulation has been shown to cause an increase in the release of CRF.

4. Discussion

Here, we have provided direct electrophysiological and immunohistochemical evidence that CRF^+ neurons in the amygdala and BnST are GABAergic. Our data provide functional

support to previous anatomical and biochemical evidence (Sun and Cassell, 1993; Dabrowska et al., 2013). These CRF^+ neurons, which are critical for the response to both acute and chronic adversity (Walker and Davis, 2008; Walker et al., 2009; Luthi and Luscher, 2014), have been associated with the control of anxiety-like responses within the extended amygdala (Davis et al., 2010). A similar role for GABAergic neurons in the amygdala has been described, for example, the facilitation of the expression of fear learning through disinhibition (Wolff et al., 2014). Here, we have shown that these two populations of neurons (GABA and CRF) are highly overlapping.

The pattern of expression of tdTomato CRF^+ neurons we detected is consistent with that previously reported in the PVN, CeA and BnST (Silberman et al., 2013; Wamsteeker Cusulin et al., 2013; Chen et al., 2015) and is consistent with decades of histological characterization of CRF expression patterns. Within the BnST and the CeA, tdTomato/CRF^+ neurons form a longitudinal group of cells in horizontal slices that appear as a cluster of high density neurons in coronal slices. This high density of fluorescent signal greatly assists with the localization of these neurons. Our immunohistochemical evidence supports the findings showing that CRF^+ neurons in *crf*-Cre mice are CRF immunopositive and express tdTomato (Wamsteeker Cusulin et al., 2013; Chen et al., 2015). CRF^+ neurons in CeA have similar soma size and electrophysiological characterization of the action potential firing patterns reveals fewer subtypes compared to the more complex varieties found in BnST (Dabrowska et al., 2013; Silberman et al., 2013).

Here, we employed the optogenetic approach, which has been recently utilized to examine neural circuitry controlling anxiety (Johansen et al., 2012; Sparta et al., 2013). We found that ChR2 expression in CRF^+ neurons enabled robust light induced control of membrane potential and action potential firing, which was modulated by regulating light intensity. Patch clamp recordings from labeled CRF neurons and neighboring unlabeled (non-CRF) neurons during optogenetic stimulation of the field revealed the release of GABA on to the majority of CRF^- neurons in both the CeA and BnST in response to optogenetic activation of CRH neurons.

The prevalent fast synaptic action of CRF^+ neurons is GABAergic, without a strong glutamatergic component as revealed by the near complete blockade of light-evoked synaptic responses by selective GABA antagonists and the lesser effect of glutamatergic antagonists (e.g., NBQX). Indeed, the low efficacy of NBQX suggests direct connectivity between presynaptic CRF^+ neurons and their targets, without an intermediate glutamatergic synapse. Further support for the predominate GABAergic phenotype is derived from our immunohistochemistry experiments with anti-GABA antibodies. These experiments revealed extensive co-labeling of GABA and tdTomato (as a marker of CRF^+ neurons) in the CeM but not in nearby CeL.

In addition to the striking GABAergic innervation of CRF^- neurons by CRF^+ neurons, a fraction of CRF^+ neurons also receive GABAergic innervation from CRF^+ neuron collaterals. This pattern reveals a complex reciprocal synaptic connectivity within the CeA and BnST. This is reminiscent of negative feedback microcircuit regulation in the dorsal striatum (Plenz, 2003). While it is plausible that GABAergic synaptic connectivity amongst

CRF neurons occurs within each brain region of interest, it is also clear from numerous prior studies that CRF neurons can send long-range projections to other brain regions. For example, CRF neurons in the amygdala can project to the BnST, and CRF neurons in the nucleus of the solitary tract project to the parabrachial nucleus (Swanson et al., 1983; Herbert and Saper, 1990; Gray, 1993). This presents the possibility that reciprocal optogenetic activation results from synaptic terminals deriving from one of these regions. This will need to be investigated systematically with targeted virus injection studies.

CRF-R1 receptors, one of two subtypes of CRF receptors are found throughout the brain. Interestingly, they are found on CRF neurons in the PVN (Imaki et al., 2001), and have also been reported in CRF^+ neurons in the CeA (Beckerman et al., 2013). Recently, it has been reported that within CeA, genetically identifiable CRF receptor type 1, CRF-R1-$eGFP^+$ expressing neurons have relatively large tonic GABAergic currents that display reduced sensitivity to THIP, the $GABA_A$ receptor δ subunit preferring agonist (Herman et al., 2013a). This study directly measured these parameters and compared them to CRF-R1 lacking neurons ($eGFP^-$). Our results suggest that many CRF^+ neurons share some of these properties with CRF-R1 neurons suggesting a partial overlap in these populations of genetically identified neurons (Beckerman et al., 2013).

CRF release in the extended amygdala has typically been associated with high-frequency, long duration firing of neurons; along with modulatory actions through G-protein coupled receptors (Rainnie et al., 1992; Yu and Shinnick-Gallagher, 1998). Our results show that the CRF-R1 antagonist, antalarmin, failed to affect light evoked IPSCs in CRF^- neurons in BnST and CeA. While long-duration light activation of CRF^+ neurons may have released CRF, the degree of neuropeptide release may have been insufficient to produce an effect detectable by blockade with antalarmin. Alternatively, light evoked GABAergic responses are not sensitive to CRF release. Future studies with bath application of CRF may be better suited to evaluate the effects of peptide signaling on CRF^+ or CRF-lacking neurons. Acute CRF application in brain slices has been shown to increase sEPSCs (Silberman et al., 2013) and sIPSCs (Oberlander and Henderson, 2012) in BnST as well as sIPSCs in CeA neurons (Nie et al., 2009). In the present study, antalarmin failed to affect sIPSCs in BnST and CeA in both control and CUS treated mice. In agreement with our results, antalarmin failed to alter sIPSC frequency in BnST neurons in control mice (Oberlander and Henderson, 2012). However, antalarmin attenuates increases in sIPSC frequency in BnST neurons in an anxiety model caused by anabolic steroids (Oberlander and Henderson, 2012). The discrepancy with our results may relate to differences between these two models of anxiety. This further supports the possibility that GABAergic responses may not be sufficiently sensitive to the endogenous CRF level in brain slices.

The key role of the BnST and CeA in the expression of responses to aversive stimuli prompted us to investigate a model of adversity that involved multiple stressors (Carvalho-Netto et al., 2011). While basal anxiety-like behavior in the open field task in the present study was high, we still were able to detect an increase in anxiety-like behavior after chronic stress. The chronic unpredictable stress paradigm significantly increased the proportion of CRF^+ neurons receiving GABAergic input from other CRF^+ neurons, as well as the strength of their synaptic connections consistent with observations of CRF neurons in the PVN

(Sarkar et al., 2011). This effect was seen in both the BnST and the CeA and it was specific for CRF^+ but not CRF^- neurons. This increased connectivity could be mediated by sprouting of GABAergic axons or by increases in quantal efficacy, but further work is required to understand the precise mechanisms. This increase in GABAergic inhibition within the extended amygdala CRF system may have functional consequences with respect to circuit output. A decrease in CeA outflow to the BnST would be expected to trigger anxiety-like responses. Indeed, chronic stress in our experiments was associated with increased anxiety-like behavior. Additionally, cell-specific deletion of the α1 subunit of the $GABA_A$ receptor in CRF neurons was shown to enhance anxiety (Gafford et al., 2012). Together with the data reported here, this is consistent with findings of Kim et al. (2013) who demonstrated that inputs from the amygdala can activate sub-regions of BnST and reduce anxiety, while inhibition of these inputs can increase anxiety (Kim et al., 2013).

5. Conclusions

Here we have shown that CRF neurons within the BnST and CeA employ GABA as a co-transmitter. These neurons send projections to both CRF^+ and CRF^- neurons within these structures. Chronic unpredictable stress selectively increased the interconnections between CRF^+ neurons and other CRF^+ neurons, and not between CRF^+ and CRF^- neurons. It is appealing to speculate that CRF neuron mediated GABAergic synaptic remodeling plays a critical role in the ability of these circuits to mediate the behavioral responses to adversity.

Acknowledgements

The authors would like to thank Niaz Sahibzada, Amanda Lewin, Ghazaul Dezfuli, and Monica Javidnia for assistance in tissue preparations for immunohistochemistry. This work was supported by the Georgetown University Dean's Pilot Award to JGP and PAF.

PAF received support from KL2TR001432.

Abbreviations:

CRF	corticotropin releasing factor
BnST	Bed nucleus of the stria terminalis
CeA	central amygdala

References

Adedoyin MO, Vicini S, Neale JH, 2010 Endogenous N-acetylaspartylglutamate (NAAG) inhibits synaptic plasticity/transmission in the amygdala in a mouse inflammatory pain model. Mol. Pain (England) 6, 60-8069-6-60.

Beckerman MA, Van Kempen TA, Justice NJ, Milner TA, Glass MJ, 2013 Corticotropin-releasing factor in the mouse central nucleus of the amygdala: ultrastructural distribution in NMDA-NR1 receptor subunit expressing neurons as well as projection neurons to the bed nucleus of the stria terminalis. Exp. Neurol. (United States) 239, 120–132.

Carvalho-Netto EF, Myers B, Jones K, Solomon MB, Herman JP, 2011 Sex differences in synaptic plasticity in stress-responsive brain regions following chronic variable stress. Physiol. Behav. (United States) 104, 242–247.

Chen Y, Molet J, Gunn BG, Ressler K, Baram TZ, 2015 Diversity of reporter expression patterns in transgenic mouse lines targeting corticotropin-releasing hormone-expressing neurons. Endocrinol. (United States) 156, 4769–4780.

Chieng BC, Christie MJ, Osborne PB, 2006 Characterization of neurons in the rat central nucleus of the amygdala: cellular physiology, morphology, and opioid sensitivity. J. Comp. Neurol. (United States) 497, 910–927.

Dabrowska J, Hazra R, Guo JD, Dewitt S, Rainnie DG, 2013 Central CRF neurons are not created equal: phenotypic differences in CRF-containing neurons of the rat paraventricular hypothalamus and the bed nucleus of the stria terminalis. Front. Neurosci. (Switzerland) 7, 156.

Daniels WM, Richter L, Stein DJ, 2004 The effects of repeated intra-amygdala CRF injections on rat behavior and HPA axis function after stress. Metab. Brain Dis. (United States) 19, 15–23.

Davis M, Walker DL, Miles L, Grillon C, 2010 Phasic vs sustained fear in rats and humans: role of the extended amygdala in fear vs anxiety. Neuropsychopharmacol. (United States) 35, 105–135.

Day HE, Curran EJ, Watson SJ Jr., Akil H, 1999 Distinct neurochemical populations in the rat central nucleus of the amygdala and bed nucleus of the stria terminalis: evidence for their selective activation by interleukin-1beta. J. Comp. Neurol. (United States) 413, 113–128.

Donatti AF, Leite-Panissi CR, 2011 Activation of corticotropin-releasing factor receptors from the basolateral or central amygdala increases the tonic immobility response in guinea pigs: an innate fear behavior. Behav. Brain Res. (Netherlands) 225, 23–30.

Fendt M, Endres T, Apfelbach R, 2003 Temporary inactivation of the bed nucleus of the stria terminalis but not of the amygdala blocks freezing induced by trimethylthiazoline, a component of fox feces. J. Neurosci. (United States) 23, 23–28.

Funk CK, O'Dell LE, Crawford EF, Koob GF, 2006 Corticotropin-releasing factor within the central nucleus of the amygdala mediates enhanced ethanol self-administration in withdrawn, ethanol-dependent rats. J. Neurosci. (United States) 26, 11324–11332.

Gafford GM, Guo JD, Flandreau EI, Hazra R, Rainnie DG, Ressler KJ, 2012 Cell-type specific deletion of GABA(A)alpha1 in corticotropin-releasing factor-containing neurons enhances anxiety and disrupts fear extinction. Proc. Natl. Acad. Sci. U. S. A. (United States) 109, 16330–16335.

Gilpin NW, 2012 Corticotropin-releasing factor (CRF) and neuropeptide Y (NPY): effects on inhibitory transmission in central amygdala, and anxiety- & alcohol-related behaviors. Alcohol. (United States) 46, 329–337.

Gray TS, 1993 Amygdaloid CRF pathways. role in autonomic, neuroendocrine, and behavioral responses to stress. Ann. N. Y. Acad. Sci. (United States) 697, 53–60.

Habib KE, Weld KP, Rice KC, Pushkas J, Champoux M, Listwak S, Webster EL, Atkinson AJ, Schulkin J, Contoreggi C, Chrousos GP, McCann SM, Suomi SJ, Higley JD, Gold PW, 2000 Oral administration of a corticotropin-releasing hormone receptor antagonist significantly attenuates behavioral, neuroendocrine, and autonomic responses to stress in primates. Proc. Natl. Acad. Sci. U. S. A. (United States) 97, 6079–6084.

Hammack SE, Mania I, Rainnie DG, 2007 Differential expression of intrinsic membrane currents in defined cell types of the anterolateral bed nucleus of the stria terminalis. J. Neurophysiol. (United States) 98, 638–656.

Hayes DM, Knapp DJ, Breese GR, Thiele TE, 2005 Comparison of basal neuropeptide Y and corticotropin releasing factor levels between the high ethanol drinking C57BL/6J and low ethanol drinking DBA/2J inbred mouse strains. Alcohol. Clin. Exp. Res. (United States) 29, 721–729.

Herbert H, Saper CB, 1990 Cholecystokinin-, galanin-, and corticotropin-releasing factor-like immunoreactive projections from the nucleus of the solitary tract to the parabrachial nucleus in the rat. J. Comp. Neurol. (United States) 293, 581–598.

Herman MA, Contet C, Justice NJ, Vale W, Roberto M, 2013a Novel subunit-specific tonic GABA currents and differential effects of ethanol in the central amygdala of CRF receptor-1 reporter mice. J. Neurosci. (United States) 33, 3284–3298.

Herman MA, Varodayan FP, Oleata CS, Luu G, Kirson D, Heilig M, Ciccocioppo R, Roberto M, 2015 Glutamatergic transmission in the central nucleus of the amygdala is selectively altered in marchigian sardinian alcohol-preferring rats: alcohol and CRF effects. Neuropharmacology 102, 21–31. [PubMed: 26519902]

Herman MA, Kallupi M, Luu G, Oleata CS, Heilig M, Koob GF, Ciccocioppo R, Roberto M, 2013b Enhanced GABAergic transmission in the central nucleus of the amygdala of genetically selected marchigian sardinian rats: alcohol and CRF effects. Neuropharmacol.(England) 67, 337–348.

Hooper A, Maguire J, 2016 Characterization of a novel subtype of hippocampal interneurons that express corticotropin-releasing hormone. Hippocampus 1, 41–53.

Hrabovszky E, Wittmann G, Turi GF, Liposits Z, Fekete C, 2005 Hypophysio-tropic thyrotropin-releasing hormone and corticotropin-releasing hormone neurons of the rat contain vesicular glutamate transporter-2. Endocrinology (United States) 146, 341–347.

Huang L, Garcia I, Jen HI, Arenkiel BR, 2013 Reciprocal connectivity between mitral cells and external plexiform layer interneurons in the mouse olfactory bulb. Front. Neural Circuits (Switzerland) 7, 32.

Ibanez-Sandoval O, Tecuapetla F, Unal B, Shah F, Koos T, Tepper JM, 2011 A novel functionally distinct subtype of striatal neuropeptide Y interneuron.J. Neurosci. (United States) 31, 16757–16769.

Imaki T, Katsumata H, Miyata M, Naruse M, Imaki J, Minami S, 2001 Expression of corticotropin releasing factor (CRF), urocortin and CRF type 1 receptors in hypothalamic-hypophyseal systems under osmotic stimulation.J. Neuroendocrinol. (England) 13, 328–338.

Jennings JH, Sparta DR, Stamatakis AM, Ung RL, Pleil KE, Kash TL, Stuber GD, 2013 Distinct extended amygdala circuits for divergent motivational states. Nat. (England) 496, 224–228.

Johansen JP, 2013 Neuroscience: anxiety is the sum of its parts. Nature (England)496, 174–175.

Johansen JP, Wolff SB, Luthi A, LeDoux JE, 2012 Controlling the elements: an optogenetic approach to understanding the neural circuits of fear. Biol. Psychiatr. (United States) 71, 1053–1060.

Kessler RC, Berglund P, Demler O, Jin R, Merikangas KR, Walters EE, 2005 Lifetime prevalence and age-of-onset distributions of DSM-IV disorders in the national comorbidity survey replication. Arch. Gen. Psychiatry (United States) 62, 593–602.

Kim SY, Adhikari A, Lee SY, Marshel JH, Kim CK, Mallory CS, Lo M, Pak S, Mattis J, Lim BK, Malenka RC, Warden MR, Neve R, Tye KM, Deisseroth K, 2013 Diverging neural pathways assemble a behavioural state from separable features in anxiety. Nature (England) 496, 219–223.

Koob GF, Thatcher-Britton K, 1985 Stimulant and anxiogenic effects of corticotropin releasing factor. Prog. Clin. Biol. Res. (United States) 192, 499–506.

Li C, Pleil KE, Stamatakis AM, Busan S, Vong L, Lowell BB, Stuber GD, Kash TL, 2012 Presynaptic inhibition of gamma-aminobutyric acid release in the bed nucleus of the stria terminalis by kappa opioid receptor signaling. Biol. Psychiatr. (United States) 71, 725–732.

Lightman SL, Young WS 3rd, 1988 Corticotrophin-releasing factor, vasopressin and pro-opiomelanocortin mRNA responses to stress and opiates in the rat. J. Physiol. (England) 403, 511–523.

Liu ZP, Song C, Wang M, He Y, Xu XB, Pan HQ, Chen WB, Peng WJ, Pan BX, 2014 Chronic stress impairs GABAergic control of amygdala through suppressing the tonic GABAA receptor currents. Mol. Brain Engl. 7, 32-6606-7-32.

Lopez de Armentia M, Sah P, 2004 Firing properties and connectivity of neurons in the rat lateral central nucleus of the amygdala. J. Neurophysiol. (United States) 92, 1285–1294.

Lowery-Gionta EG, Navarro M, Li C, Pleil KE, Rinker JA, Cox BR, Sprow GM, Kash TL, Thiele TE, 2012 Corticotropin releasing factor signaling in the central amygdala is recruited during binge-like ethanol consumption in C57BL/6J mice. J. Neurosci. (United States) 32, 3405–3413.

Luo R, Janssen MJ, Partridge JG, Vicini S, 2013 Direct and GABA-mediated indirect effects of nicotinic ACh receptor agonists on striatal neurones.J. Physiol. (England) 591, 203–217.

Luthi A, Luscher C, 2014 Pathological circuit function underlying addiction and anxiety disorders. Nat. Neurosci. (United States) 17, 1635–1643.

Ma J, Ye N, Lange N, Cohen BM, 2003 Dynorphinergic GABA neurons are a target of both typical and atypical antipsychotic drugs in the nucleus accumbens shell, central amygdaloid nucleus and thalamic central medial nucleus. Neurosci. (United States) 121, 991–998.

Madisen L, Zwingman TA, Sunkin SM, Oh SW, Zariwala HA, Gu H, Ng LL, Palmiter RD, Hawrylycz MJ, Jones AR, Lein ES, Zeng H, 2010 A robust and high-throughput cre reporting and characterization system for the whole mouse brain. Nat. Neurosci. (United States) 13, 133–140.

Madisen L, et al., 2012 A toolbox of cre-dependent optogenetic transgenic mice for light-induced activation and silencing. Nat. Neurosci. (United States) 15, 793–802.

Marchant NJ, Densmore VS, Osborne PB, 2007 Coexpression of prodynorphin and corticotrophin-releasing hormone in the rat central amygdala: evidence of two distinct endogenous opioid systems in the lateral division. J. Comp. Neurol. (United States) 504, 702–715.

Marek R, Strobel C, Bredy TW, Sah P, 2013 The amygdala and medial prefrontal cortex: partners in the fear circuit. J. Physiol. (England) 591, 2381–2391.

Masneuf S, Lowery-Gionta E, Colacicco G, Pleil KE, Li C, Crowley N, Flynn S, Holmes A, Kash T, 2014 Glutamatergic mechanisms associated with stress-induced amygdala excitability and anxiety-related behavior. Neuropharmacol. (England) 85, 190–197.

Merlo Pich E, Lorang M, Yeganeh M, Rodriguez de Fonseca F, Raber J, Koob GF, Weiss F, 1995 Increase of extracellular corticotropin-releasing factor-like immunoreactivity levels in the amygdala of awake rats during restraint stress and ethanol withdrawal as measured by microdialysis. J. Neurosci. (United States) 15, 5439–5447.

Nie Z, Zorrilla EP, Madamba SG, Rice KC, Roberto M, Siggins GR, 2009 Presynaptic CRF1 receptors mediate the ethanol enhancement of GABAergic transmission in the mouse central amygdala. Sci. J. (England) 9, 68–85.

Nijsen MJ, Croiset G, Diamant M, De Wied D, Wiegant VM, 2001 CRH signalling in the bed nucleus of the stria terminalis is involved in stress-induced cardiac vagal activation in conscious rats. Neuropsychopharmacol. (United States) 24, 1–10.

Oberlander JG, Henderson LP, 2012 Corticotropin-releasing factor modulation of forebrain GABAergic transmission has a pivotal role in the expression of anabolic steroid-induced anxiety in the female mouse. Neuropsychopharmacol. (England) 37, 1483–1499.

Padival M, Quinette D, Rosenkranz JA, 2013 Effects of repeated stress on excitatory drive of basal amygdala neurons in vivo. Neuropsychopharmacol. (England) 38, 1748–1762.

Partridge JG, Lewin AE, Yasko JR, Vicini S, 2014 Contrasting actions of group I metabotropic glutamate receptors in distinct mouse striatal neurones. J. Physiol. (England) 592, 2721–2733.

Pitts MW, Todorovic C, Blank T, Takahashi LK, 2009 The central nucleus of the amygdala and corticotropin-releasing factor: insights into contextual fear memory. J. Neurosci. (United States) 29, 7379–7388.

Plenz D, 2003 When inhibition goes incognito: feedback interaction between spiny projection neurons in striatal function. Trends Neurosci. (England) 26, 436–443.

Rainnie DG, Fernhout BJ, Shinnick-Gallagher P, 1992 Differential actions of corticotropin releasing factor on basolateral and central amygdaloid neurones, in vitro. J. Pharmacol. Exp. Ther. (United States) 263, 846–858.

Richter RM, Zorrilla EP, Basso AM, Koob GF, Weiss F, 2000 Altered amygdalar CRF release and increased anxiety-like behavior in sardinian alcohol-preferring rats: a microdialysis and behavioral study. Alcohol. Clin. Exp. Res. (United States) 24, 1765–1772.

Sahuque LL, Kullberg EF, Mcgeehan AJ, Kinder JR, Hicks MP, Blanton MG, Janak PH, Olive MF, 2006 Anxiogenic and aversive effects of corticotropin-releasing factor (CRF) in the bed nucleus of the stria terminalis in the rat: role of CRF receptor subtypes. Psychopharmacol. Berl.(Germany) 186, 122–132.

Sakanaka M, Shibasaki T, Lederis K, 1986 Distribution and efferent projections of corticotropin-releasing factor-like immunoreactivity in the rat amygdaloid complex. Brain Res.(Netherlands) 382, 213–238.

Sandi C, Cordero MI, Ugolini A, Varea E, Caberlotto L, Large CH, 2008 Chronic stress-induced alterations in amygdala responsiveness and behavior–modulation by trait anxiety and corticotropin-releasing factor systems. Eur. Neurosci. (France) 28, 1836–1848.

Sarkar J, Wakefield S, MacKenzie G, Moss SJ, Maguire J, 2011 Neurosteroido-genesis is required for the physiological response to stress: role of neurosteroid-sensitive GABAA receptors. J. Neurosci. (United States) 31, 18198–18210.

Sawchenko PE, Swanson LW, Vale WW, 1984 Corticotropin-releasing factor: Co-expression within distinct subsets of oxytocin-, vasopressin-, and neurotensin-immunoreactive neurons in the hypothalamus of the male rat.J. Neurosci. (United States) 4, 1118–1129.

Schulkin J, 2011 Evolutionary conservation of glucocorticoids and corticotropin releasing hormone: behavioral and physiological adaptations. Brain Res. (Netherlands) 1392, 27–46.

Schweizer MC, Henniger MS, Sillaber I, 2009 Chronic mild stress (CMS) in mice: of anhedonia, 'anomalous anxiolysis' and activity. PLoS One (United States) 4, e4326.

Silberman Y, Winder DG, 2013 Emerging role for corticotropin releasing factor signaling in the bed nucleus of the stria terminalis at the intersection of stress and reward. Front. Psychiatr. Switzerl 4, 42.

Silberman Y, Matthews RT, Winder DG, 2013 A corticotropin releasing factor pathway for ethanol regulation of the ventral tegmental area in the bed nucleus of the stria terminalis. J. Neurosci. (United States) 33, 950–960.

Sparta DR, Jennings JH, Ung RL, Stuber GD, 2013 Optogenetic strategies to investigate neural circuitry engaged by stress. Behav. Brain Res. Neth 255, 19–25.

Sterrenburg L, Gaszner B, Boerrigter J, Santbergen L, Bramini M, Roubos EW, Peeters BW, Kozicz T, 2012 Sex-dependent and differential responses to acute restraint stress of corticotropin-releasing factor-producing neurons in the rat paraventricular nucleus, central amygdala, and bed nucleus of the stria terminalis. J. Neurosci. Res. (United States) 90, 179–192.

Sun N, Cassell MD, 1993 Intrinsic GABAergic neurons in the rat central extended amygdala. J. Comp. Neurol. (United States) 330, 381–404.

Swanson LW, Sawchenko PE, Rivier J, Vale WW, 1983 Organization of ovine corticotropin-releasing factor immunoreactive cells and fibers in the rat brain: an immunohistochemical study. Neuroendocrinology (Switzerland) 36, 165–186.

Taniguchi H, He M, Wu P, Kim S, Paik R, Sugino K, Kvitsiani D, Fu Y, Lu J, Lin Y, Miyoshi G, Shima Y, Fishell G, Nelson SB, Huang ZJ, 2011 A resource of cre driver lines for genetic targeting of GABAergic neurons in cerebral cortex. Neuron (United States) 71, 995–1013.

Valentino RJ, Page M, Van Bockstaele E, Aston-Jones G, 1992 Corticotropin-releasing factor innervation of the locus coeruleus region: distribution of fibers and sources of input. Neuroscience (England) 48, 689–705.

Valentino RJ, Rudoy C, Saunders A, Liu XB, Van Bockstaele EJ, 2001 Corticotropin-releasing factor is preferentially colocalized with excitatory rather than inhibitory amino acids in axon terminals in the peri-locus coeruleus region. Neuroscience (United States) 106, 375–384.

Walker D, Yang Y, Ratti E, Corsi M, Trist D, Davis M, 2009 Differential effects of the CRF-R1 antagonist GSK876008 on fear-potentiated, light- and CRF-enhanced startle suggest preferential involvement in sustained vs phasic threat responses. Neuropsychopharmacol. (United States) 34, 1533–1542.

Walker DL, Davis M, 2008 Role of the extended amygdala in short-duration versus sustained fear: a tribute to dr. lennart heimer. Brain Struct. Funct. (Germany). 213, 29–42.

Wamsteeker Cusulin JI, Fuzesi T, Watts AG, Bains JS, 2013 Characterization of corticotropin-releasing hormone neurons in the paraventricular nucleus of the hypothalamus of crh-IRES-cre mutant mice. PLoS One (United States) 8, e64943.

Washington PM, Forcelli PA, Wilkins T, Zapple DN, Parsadanian M, Burns MP, 2012 The effect of injury severity on behavior: a phenotypic study of cognitive and emotional deficits after mild, moderate, and severe controlled cortical impact injury in mice. J. Neurotrauma (United States) 29, 2283–2296.

Wolff SB, Grundemann J, Tovote P, Krabbe S, Jacobson GA, Muller C, Herry C, Ehrlich I, Friedrich RW, Letzkus JJ, Luthi A, 2014 Amygdala interneuron subtypes control fear learning through disinhibition. Nature (England) 509, 453–458.

Wurzman R, Forcelli PA, Griffey CJ, Kromer LF, 2015 Repetitive grooming and sensorimotor abnormalities in an ephrin-A knockout model for autism spectrum disorders. Behav. Brain Res. 278, 115–128. [PubMed: 25281279]

Yu B, Shinnick-Gallagher P, 1998 Corticotropin-releasing factor increases dihydropyridine- and neurotoxin-resistant calcium currents in neurons of the central amygdala. J. Pharmacol. Exp. Ther. (United States) 284, 170–179.

Zorrilla EP, Logrip ML, Koob GF, 2014 Corticotropin releasing factor: a key role in the neurobiology of addiction. Front. Neuroendocrinol. (United States) 35, 234–244.

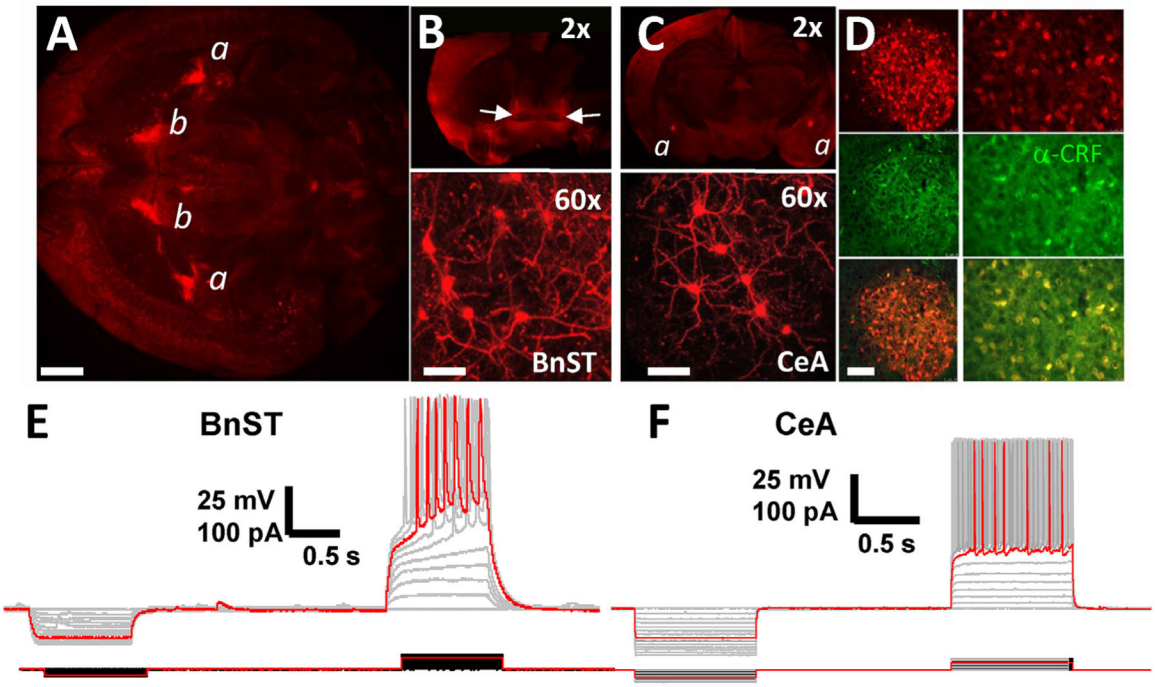

Fig. 1.

crf;tdTomato neurons in BnST and CeA. (**A**) Low magnification image illustrating the high expression of red fluorescent CRF^{+} neurons in BnST (*b*) and the CeA (*a*) in a horizontal section. Scale bar 1 mm. (**B**) Low magnification (2×) image illustrating the extent of red fluorescent CRF^{+} neurons in a coronal sections containing the anterior commissure (*white arrows*) to identify the location of the BnST. (**C**) Low magnification (2×) image illustrating the extent of red fluorescent CRF^{+} neurons in a more caudal section containing the amygdala (*a*). The lower panels in B and C illustrate at a higher magnification (60×) neurons in the respective areas. Scale bars 1.6 mm (*top*) 25 μm (*bottom*). (**D**) Immunodetection of CRF in CeA neurons expressing tdTomato. Anatomical distribution is compared between *CRF* mediated tdTomato expression (*red*, *top*), anti-CRF antibody staining (*green*, *middle*) and merged images (*yellow*, *bottom*). The left panels are low power images, and on the right are the same areas at increased magnification. Scale bars 100 (left) & 50 μm (right). Current clamp recordings from visually identified CRF^{+} neurons in the BnST (**E**) and CeA (**F**). Superimposed voltage responses to hyperpolarizing and depolarizing current injections illustrate the intrinsic membrane properties and the firing pattern of CeA and BnST. Red traces highlight contrasting firing patterns.

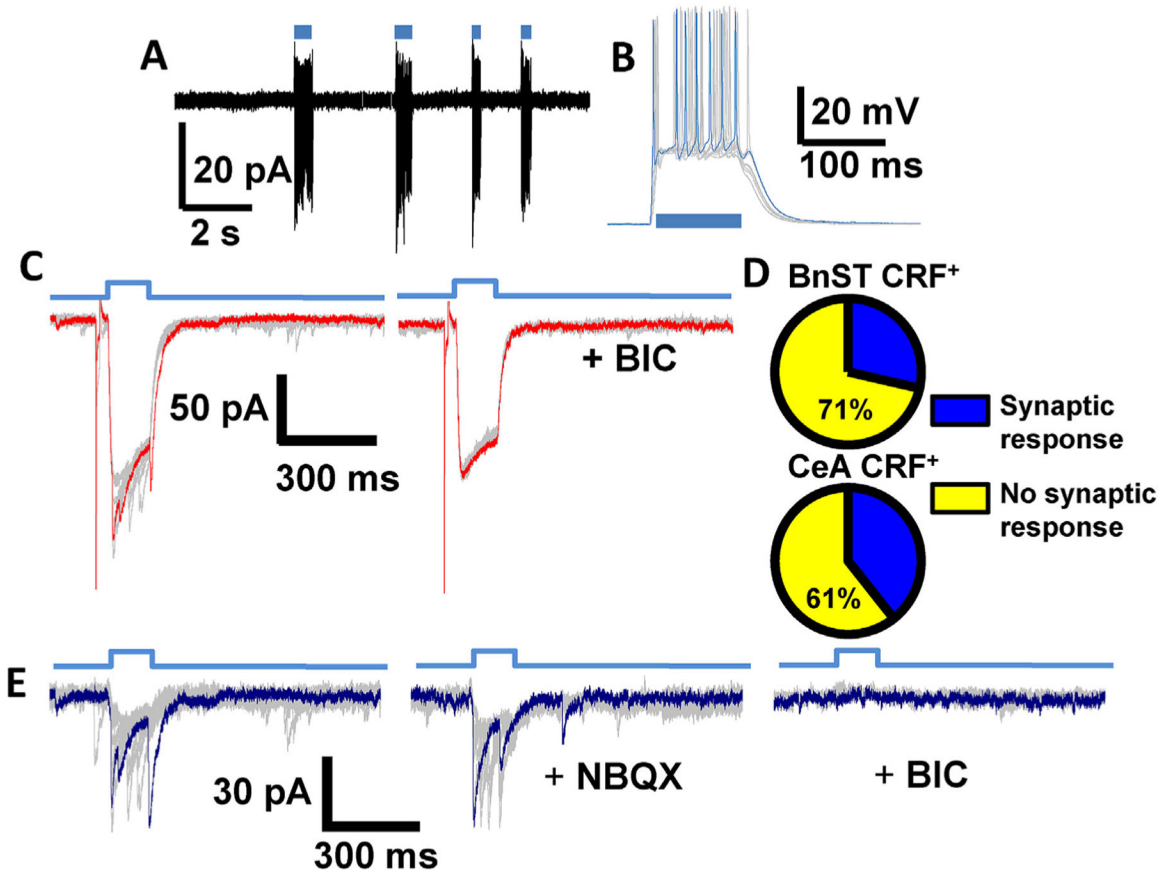

Fig. 2.

crf;ChR2-YFP neurons are photo-active and release GABA. (**A**) Optogenetic activation of CRF^+ neurons in the CeA shows that sequential pulses of light (*blue horizontal bars*) consistently evoked sustained action potential firing in a cell-attached recording. (**B**) Light activation induced sustained depolarizations (superimposed *gray* traces, example trace in *blue*) leading to action potentials in current clamp. (**C**) Light activation (time course shown in top *blue trace*) also induced fast inward currents (superimposed *gray* traces, example trace in *red*) recorded with a high $[Cl^-]_i$ pipette solution in voltage clamp. Application of 25 μM BIC (*right traces*) in the same cell revealed an isolated ChR2 current. The response to a preceding 5 mV test pulse used to monitor access and input resistance is also shown. (**D**) Pie chart depicting the percentage of synaptically responsive CRF^+ neurons (blue wedge) in BnST (top) and CeA (bottom). Unconnected CRF^+ neurons are shown in yellow. (**E**) Superimposed light evoked IPSCs (*gray*, example in *blue*) obtained by subtraction of the average ChR2 current in BIC and shown in the absence (*left*), the presence of NBQX (5 μM, *center*) and BIC (*right*).

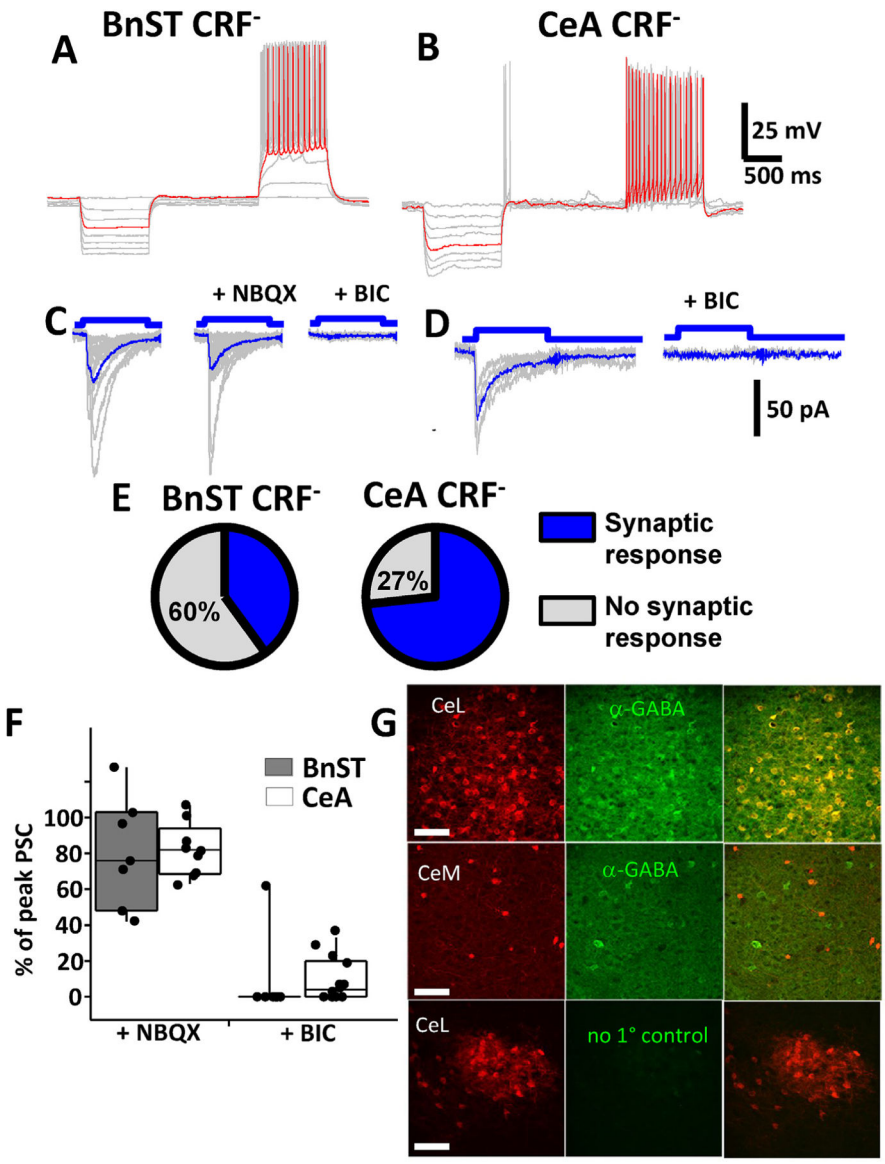

Fig. 3.

Optogenetic activation of GABAergic currents in unidentified CRF⁻ lacking neurons. Current clamp recordings from an unlabeled neuron in the BnST (**A**) or CeA (**B**) from a *crf*;ChR2-YFP mouse. Shown are voltage responses to 10 pA hyperpolarizing and depolarizing current injection steps highlighting the differences in firing patterns of these neurons (superimposed *gray* traces, example trace in *red*). Voltage clamp recordings (superimposed *gray* traces, average *blue* trace) of light evoked (100 ms pulse) postsynaptic currents in the absence and presence of 5 μM NBQX or 25 μM BIC in a CRF⁻ neuron in BnST (**C**) or 25 μM BIC in CeA (**D**). (**E**) Pie chart depicting the percentage of synaptically responsive CRF⁻ neurons (blue wedge) in BnST (left) and CeA (right). Unresponsive CRF⁻ neurons are depicted in gray. Summary box and whisker plots comparing the pharmacological effects on the % inhibitory effect of NBQX (left) or BIC (right) on light evoked postsynaptic currents (PSC) from BnST (gray bars) or CeA (white bars) (**F**).

Immuno-detection of GABA in CRF^{+} neurons expressing td-Tomato (**G**). Anatomical distribution is compared between *crf*-mediated tdTomato expression (*red*, *left*), anti-GABA antibody staining (*green*, *middle*) and merged images (*yellow*, *right*). The *top* panels are from CeL while the *middle* panels are from nearby CeM. The bottom panels are control immunostaining lacking primary antibodies from CeL. Scale bars 100 μm.

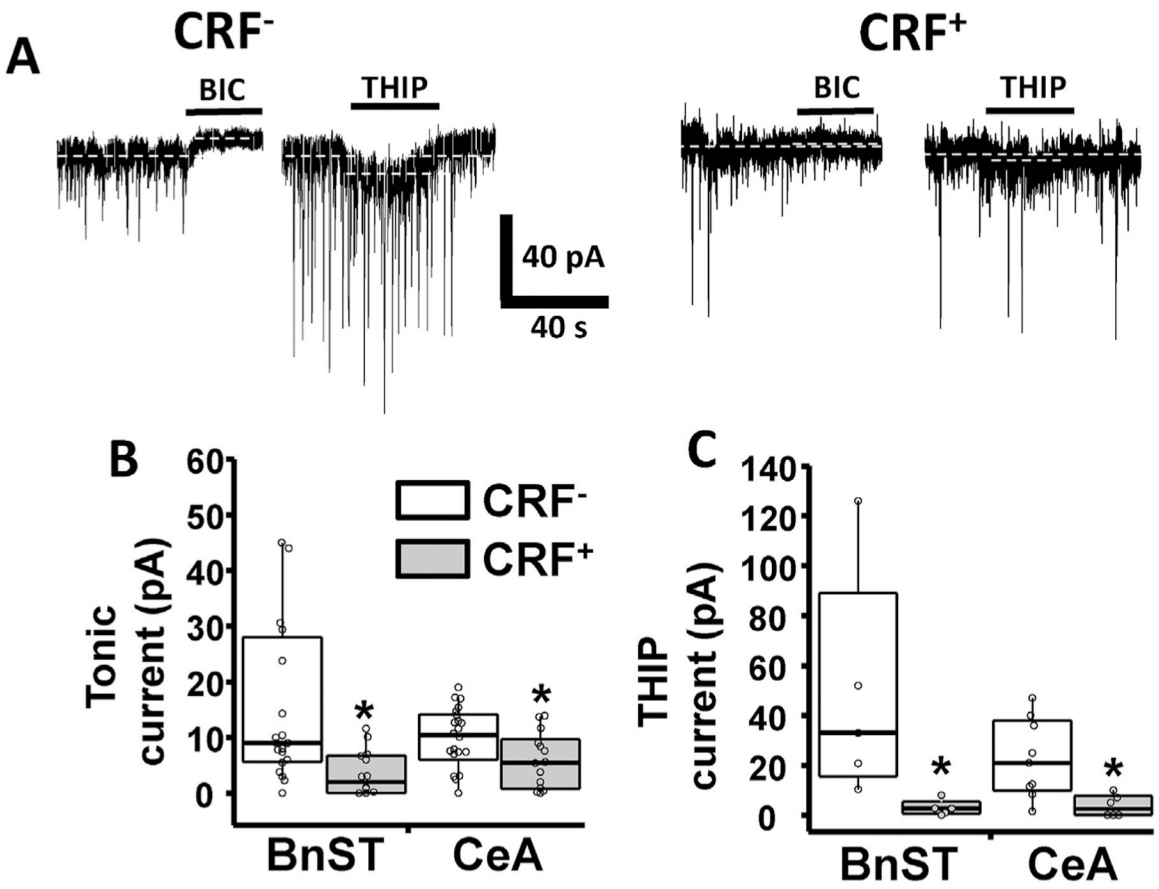

Fig. 4.

$GABA_A$ mediated tonic currents in BnST and CeA neurons. (**A**) Example voltage clamp recordings from unidentified CRF^- lacking neurons and visually identified CRF^+ neurons in the CeA illustrating spontaneous inhibitory postsynaptic currents (sIPSCs) and the occurrence of tonic GABAergic conductance. The $GABA_A$ receptor antagonist BIC (25 μM) abolished sIPSCs and revealed tonic current. The extrasynaptic $GABA_A$ receptor preferring agonist THIP (1 μM) differentially increased tonic current. Summary box and whisker plots comparing the pharmacological effects of BIC (**B**) and THIP sensitive current (**C**). White bars are recordings from CRF^- lacking neurons while the gray bars are recordings from CRF^+ neurons. *, $p < 0.05$, Mann-Whitney test.

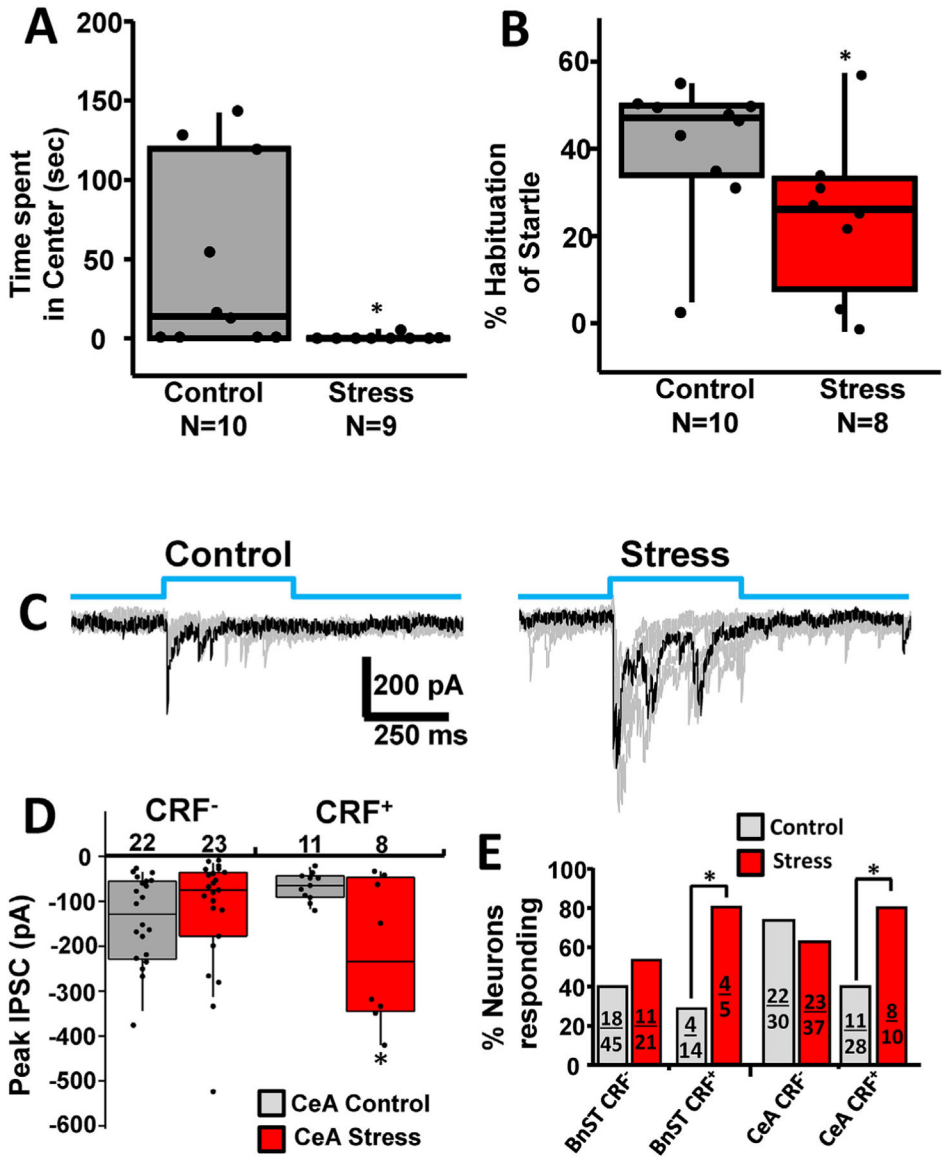

Fig. 5.

Chronic Unpredictable Stress induces anxiety-like behavior in wild type mice and affects synaptic connectivity in CRF$^+$ neurons in BnST and CeA. (**A**) Two days after cessation of chronic stress (consistent with the timing used in our electrophysiological experiments), stressed animals showed increased anxiety-like behavior in the open field. This is evident in a significant decrease in the time spent in the center of the arena. *$p < 0.05$, Mann-Whitney test. (**B**) Two weeks after cessation of chronic stress, anxiety-like behavior was assessed by habituation to acoustic startle (120 dB white noise). Animals exposed to chronic unpredictable stress displayed significantly less habituation of the acoustic startle response. *, $p < 0.05$, Mann-Whitney test.(**C**) Delivery of blue light (*top*, *blue* steps) evoked IPSCs from a CRF$^+$ neuron from a control (*left*) and a stressed animal (*right*). Superimposed multiple trial traces are shown in *gray* and example traces in *black*. (**D**) Summary box and whisker plots comparing the peak IPSC from control (*gray*) and stressed (*red*) neurons for

400 ms blue pulses. (**E**) Chi-square analysis of the % neurons responding to light with PSCs are shown in control (*gray*) or stressed (*red*) conditions. Fractions inside each bar correspond to the number of responding neurons (*numerator*) over the total number of cells recorded (*denominator*). *, $p < 0.05$.

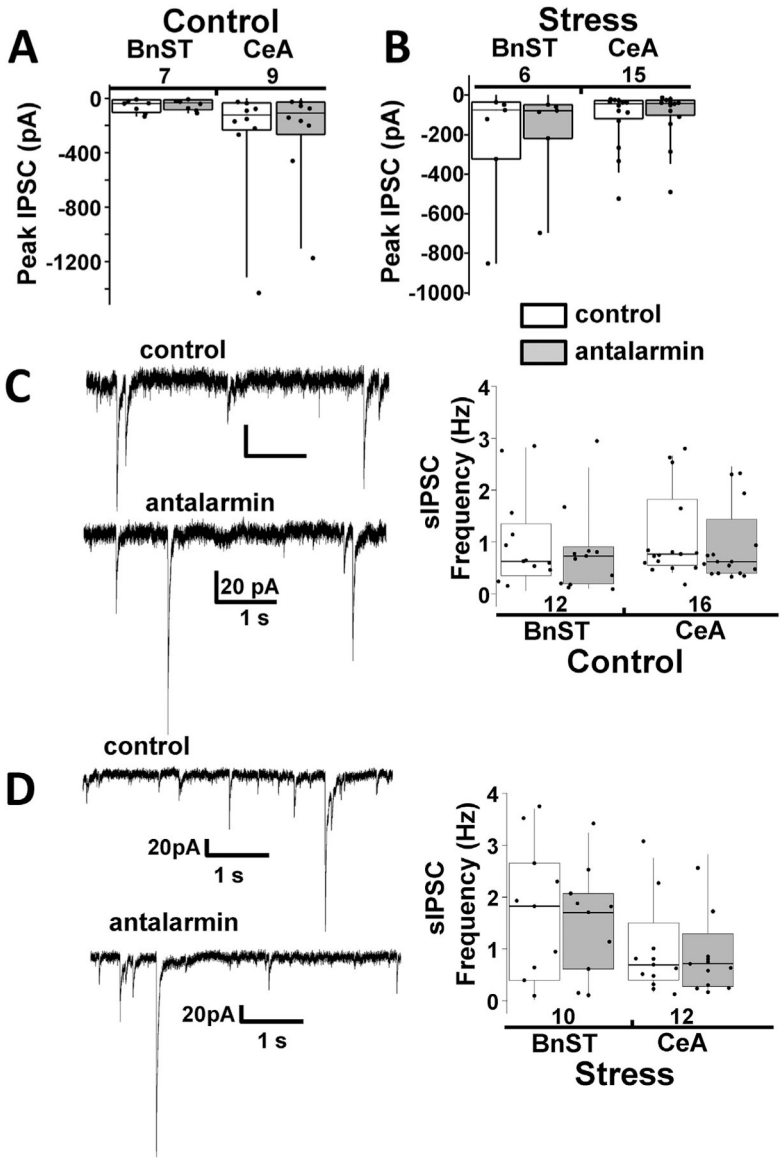

Fig. 6.

CRF R1 receptor antagonists do not significantly affect spontaneous IPSCs in control or stressed mice (**A**) Summary box and whisker plots comparing the peak IPSC in the absence (control, *white*) and presence (*gray*) of 25 μM antalarmin, a CRF receptor antagonist, for 400 ms light evoked IPSCs from CRF⁻ neurons from the BnST (*left*) or CeA (*right*). (**B**) Same data plotted from CRF⁻ lacking neurons exposed to stress protocols. The numbers below the brain region description indicate number of neurons tested. (**C**) Example voltage clamp recordings (left) from unidentified CRF⁻ lacking neurons in the BnST illustrating spontaneous inhibitory postsynaptic currents (sIPSCs) in the absence (*control*) and presence of a CRF R1 antagonist (*antalarmin*). Summary box and whisker plots (right) comparing the lack of a pharmacological effect in BnST and CeA. (**D**) Same data plotted from CRF⁻

lacking neurons exposed to stress protocols. The numbers above the brain region description indicate number of neurons tested.